

Coherent anti-Stokes Raman spectroscopy for nano-imaging with a metallic near-field probe

Satoshi Kawata,^{1,4,5} Taro Ichimura,^{2,5} Norihiko Hayazawa,^{4,5}
Mamoru Hashimoto,^{3,5} and Yasushi Inouye^{2,4,5}

¹ Department of Applied Physics, Osaka University, Suita, Osaka 565-0871, Japan

² Graduate School of Frontier Biosciences, Osaka University, Suita, Osaka 565-0871, Japan

³ Department of mechanical engineering and bioengineering, Osaka University, Toyonaka, Osaka
560-8531, Japan

⁴ RIKEN, Wako, Saitama 351-0198, Japan

⁵ CREST, JST, Japan

ABSTRACT

A metallic nano-probe has locally induced coherent anti-Stokes Raman scattering (CARS) of adenine molecules in a nanometric DNA network structure. The excitation fields and CARS polarization are enhanced by the tip apex of the nano-probe through the excitation of local surface plasmons. Owing to the third-order nonlinearity, the excitation of the CARS polarization is extremely confined to the end of the tip apex, resulting in the spatial resolution far beyond the diffraction limit of light. Our CARS microscope using a silver-coated probe visualized the DNA network structure at a specific vibrational frequency ($\sim 1337\text{ cm}^{-1}$) of adenine molecules with a spatial resolution of $\sim 15\text{ nm}$ and sufficient sensitivity.

1. INTRODUCTION

An optical microscope with nanometric spatial resolution is a preferable tool for advances of nanotechnology and nanoscience, because a variety of spectroscopic techniques that provide rich information on materials can be incorporated in the optical microscopy. Optical photon in the visible region is moderate to soft materials so that it is widely applicable to many types of nanomaterials and biomolecules. Near field scanning optical microscopy (NSOM) using an apertureless metallic probe tip has realized optical sensing with high spatial resolution beyond the diffraction limit of light [1]. The essential feature of the apertureless NSOM is the use of the electric field enhancement effect by the metallic tip. The field enhancement effect is attributed to the excitation of the local mode of the surface plasmon polaritons (tip-plasmon) as well as the singular behavior of the non-retarded field (lightning-rod effect) [2]. After the innovation of the apertureless NSOM, many scientists applied the field enhancement effect to amplification of light emission due to quantum interaction such as fluorescence [3,4], two-photon-excited fluorescence [5], infrared absorption [6,7,8], and Raman scattering [9-15]. In particular, the tip-enhancement of Raman scattering allows for nano-scale vibrational spectroscopy, hence it is the promising tools that acquire chemical information on molecular species and conformation of nano devices with nano-scaled spatial resolution.

In order to circumvent the problems of extremely small signals in nano-scaled spectroscopic sensing, in the current work

we combine coherent anti-Stokes Raman scattering (CARS) spectroscopy, one of third-order coherent nonlinear Raman scatterings [16,17], with the field enhancement effect of a metallic tip [18-20]. The third-order polarization of CARS is locally induced by the plasmonic field near the metallic tip. This technique allows for molecular vibration imaging because CARS spectroscopy provides the same spectroscopic information as ordinary spontaneous Raman spectroscopy. The excitation of CARS polarization can be further confined spatially and highly enhanced at the very end of the probe tip owing to its third-order nonlinearity, providing higher spatial resolution than tip-enhanced spontaneous Raman scattering. Compared to the alternative type of NSOM using an aperture-type probe, which was previously combined with CARS spectroscopy [21], the use of tip-enhancement effect is more advantageous with respect to spatial resolution, and is indispensable for observation of small number of molecules. We realized tip-enhanced CARS imaging of a specific vibrational mode of DNA molecules in the fingerprint region with a spatial resolution of ~ 15 nm and very high sensitivity [20].

2. PLASMONIC ENHANCEMENT OF CARS

CARS spectroscopy uses three incident fields including a pump field (ω_1), a Stokes field (ω_2 ; $\omega_2 < \omega_1$), and a probe field (ω_3), and induces a nonlinear polarization at the frequency of $\omega_{\text{CARS}} = 2\omega_1 - \omega_2$, as shown in Fig. 1(a). When the frequency difference of ω_1 and ω_2 ($\omega_1 - \omega_2$) coincides with one of specific molecular vibrational frequencies (Ω_{Raman}) of Raman-active modes of a given sample, the anti-Stokes Raman signal is resonantly generated [17]. Recently several scientists have reported that tight focusing of the excitation fields with a high numerical aperture (NA) objective lens can achieve CARS microscopy with three-dimensional imaging capability at a submicron scale [22,23]. The phase matching condition can be satisfied automatically in the focused fields of multiple angles [24]. In other words, the phase matching condition is not necessary to consider when the CARS polarizations are generated only in a volume smaller than the propagation wavelength of CARS light [25,26]. In our previous work, CARS was strongly amplified by isolated gold nanoparticles, which verified the possibility of the local enhancement of CARS by a metallic nano-structure [27]. Based on the concept mentioned above, one can observe CARS signals generated by the enhanced electric field at a metallic tip end of nanometric scale.

Figure 1(b) shows a schematic illustration of CARS generation by a metallic probe tip. Both the incident fields (ω_1 and ω_2)

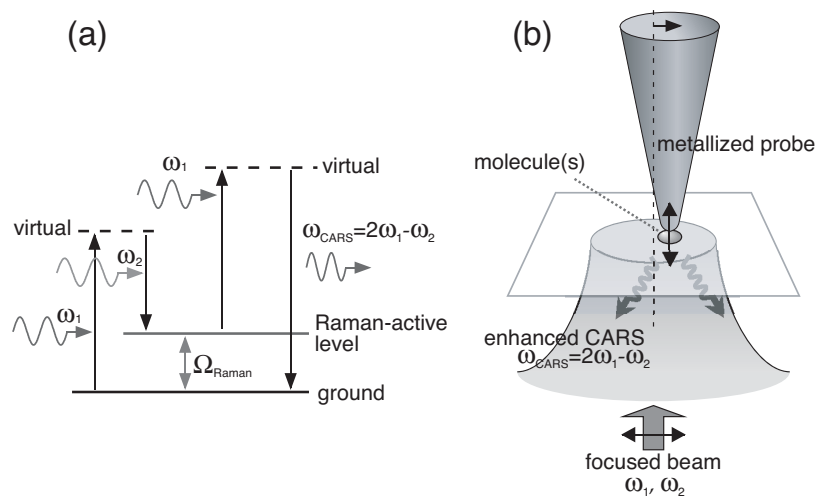


Fig. 1. (a) Energy diagram of the CARS process. (b) Schematic illustration of the local enhancement of CARS by a metallic tip.

) are strongly amplified by the metallic tip in the tightly focused spot, and induce CARS polarization with $\omega_{\text{CARS}} = 2\omega_1 - \omega_2$ in the molecules located near the tip. As the z -polarized component of the electric field along the tip axis is dominant in the tip-enhanced local field [28,29], the CARS polarizations are induced along the z -direction. For effective coupling of incident fields and the local fields, the tip has to be in a position where the incident electric field in the z -direction is strong. Since linearly polarized beams are used, the peaks of the z -component are found at ~ 200 nm from the center of the focused spot in the direction parallel to the polarization of the incident fields (Fig. 2). Thus, the tip is displaced to one of the peaks, as shown in Fig. 2(a). The CARS polarizations of molecules are locally generated within the very small volume near the tip so that the ensemble of the induced polarizations behaves as a dipole oscillating in the z -direction. The backscattered component of CARS can be efficiently collected with the high NA focusing lens. Scanning the sample stage, while keeping the tip at the focused spot, can acquire two-dimensional tip-enhanced CARS images of a specific vibrational mode with a high spatial resolution that is determined by the size of the tip end rather than the diffraction limited focused spot.

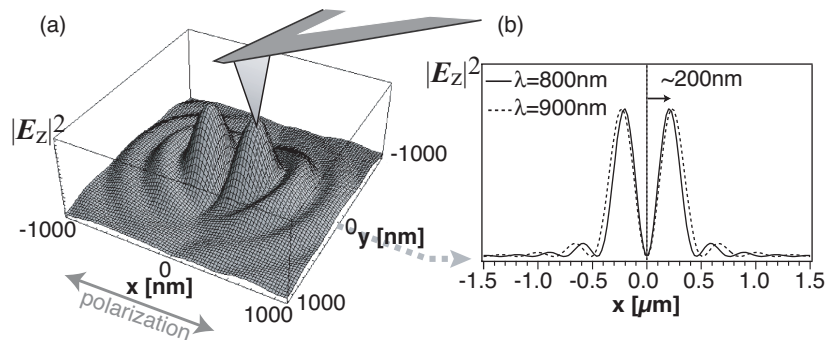


Fig. 2. Tip positioning for effective coupling with the z component of the electric field. (a) Calculated two dimensional profile of the light intensity of z -polarized component. (b) One dimensional profiles calculated for two wavelengths, 800 nm and 900 nm.

3. EXPERIMENTAL SYSTEM

The experimental system of the CARS microscopy is shown in Fig. 3. The system mainly consists of two mode-locked Ti:sapphire lasers (Spectra Physics, Tsunami, pulse duration ~ 5 ps, spectral band width ~ 4 cm^{-1} , repetition rate: 80 MHz), an inverted optical microscope (NIKON, TE300), and an atomic force microscope (Park Scientific Instruments, Bio Probe) using a silicon cantilever tip coated with 20nm-thick silver film [12-14]. The ω_1 and ω_2 beams are collinearly overlapped in time and space, and introduced into the microscope with an oil-immersion objective lens (NA = 1.4) focused onto the sample surface. The AFM-controlled probe tip contacts the sample surface with the constant force and is illuminated by the focused spot. The repetition rate of the excitation lasers is controlled by an electro-optically (EO) modulated pulse picker (Conoptics, 350-160) and a pre-compensation system of polarization with the combination of a polarization prism and a quarter wave plate. The pulse picker assisted by the pre-compensation system achieves an extinction ratio of up to approximately 200 for both beams with one EO modulator. The backscattered CARS emission is collected with the same objective lens and detected with an avalanche-photo-diode (APD) based photon-counting module (Perkin Elmer, SPCM-AQ-14) through an excitation-cut filter and a monochromator (Acton, $f = 300$ mm). The observing spectral width through the detection system is ~ 12 cm^{-1} . The pulse signals from the APD are counted by a gated photon counter (Stanford Research Systems, SR400) synchronously triggered with the pulse picker. The dark counts are effectively reduced to ~ 0 counts/sec with the gate width of 5 ns. The repetition rate was reduced to 800 kHz to avoid the thermal damage on both the sample and the silver tip while keeping the peak power high.

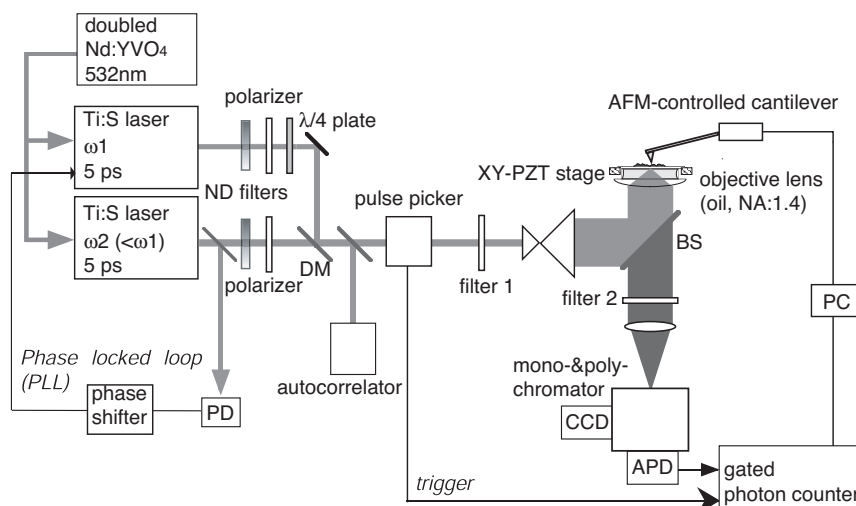


Fig. 3. Experimental setup for the tip-enhanced CARS microscopy. See the text for detail.

4. CARS IMAGING OF DNA MOLECULES

We used DNA molecules of poly(dA-dT) aggregated into clusters for CARS imaging. The poly(dA-dT) solution in water (250 $\mu\text{g/ml}$) is cast and dried on a coverslip in the room temperature with the fixation time of ~ 24 hours. The dimensions of the clusters are typically ~ 20 nm in height and ~ 100 nm in width. The frequency difference of the two excitation lasers for CARS imaging was set to be 1337 cm^{-1} corresponding to a Raman mode of adenine (ring breathing mode of diazole) by tuning the excitation frequencies ω_1 and ω_2 to be 12710 cm^{-1} (λ_1 : 786.77 nm) and 11373 cm^{-1} (λ_2 : 879.25 nm), respectively [30]. After the ‘on-resonant’ imaging, the frequency of ω_2 was changed such that the frequency difference corresponds to none of Raman-active vibration (‘off-resonant’). Figure 4 shows a spontaneous Stokes Raman spectrum of the DNA in a part of the fingerprint region. The solid arrows on the spectrum denote the frequencies adopted for the ‘on-resonant’ and ‘off-resonant’ conditions in CARS imaging.

Figure 5 shows the CARS images of the DNA clusters obtained by our system. Figures 5(a) and (b) are the tip-enhanced CARS image at the on-resonant frequency (1337 cm^{-1}) and the simultaneously acquired topographic AFM image. The

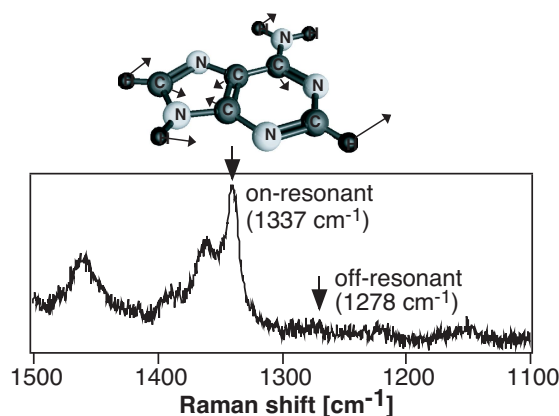


Fig. 4. A spontaneous Raman spectrum of the DNA of poly(dA-dT).poly(dA-dT). The two frequencies adopted for our CARS imaging are indicated by the downward arrows. The on-resonant frequency at 1337 cm^{-1} can be assigned to the ring-breathing mode of diazole adenine molecule in the DNA.

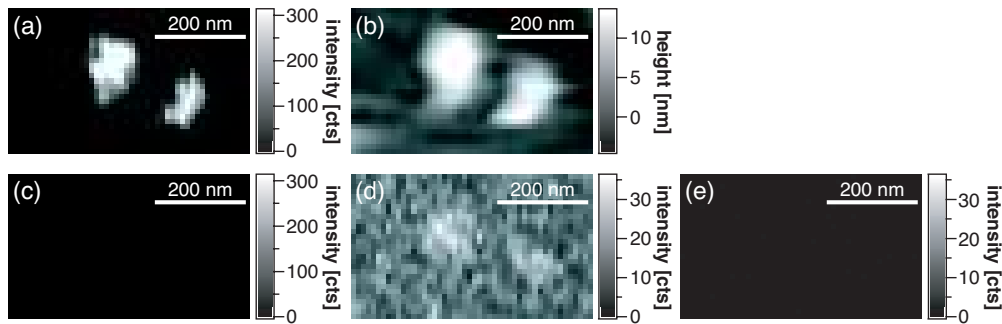


Fig. 5. CARS images of the DNA clusters. (a) Tip-enhanced CARS image at on-resonant frequency (1337 cm^{-1}), and (b) the simultaneously obtained topographic image. (c) Tip-enhanced CARS image at the off-resonant frequency (1278 cm^{-1}). (d) The same image as (c) shown with a different gray scale. (e) CARS image of the corresponding area obtained without the silver tip. The scanned area is 500 nm by 300 nm . The number of photons counted in 100 ms was recorded for one pixel. The acquisition time was ~ 3 minutes for the image. The average powers of the ω_1 and ω_2 beams were $30\text{ }\mu\text{W}$ and $15\text{ }\mu\text{W}$ at the 800 kHz repetition rate.

DNA clusters of $\sim 100\text{ nm}$ diameter are visualized in Fig. 5(a). The two DNA clusters with distance of $\sim 160\text{ nm}$ are obviously distinguished by the tip-enhanced CARS imaging. This indicates that the CARS imaging successfully achieved super-resolving capability beyond the diffraction limit of light. At the off-resonant frequency (1278 cm^{-1}), the CARS signals mostly vanished in Fig. 5(c). Figures 5(a) and (c) verify that vibrationally resonant CARS is emitted from the DNA molecules at the specific frequency. However, there remains some slight signal increase at the clusters at the off-resonant frequency, as seen in Fig. 5(d) which is the same as Fig. 5(c) but is shown with a different gray scale. This can be caused by both the frequency-invariant (non-resonant) component of the nonlinear susceptibility of DNA [17] and the topographic artifact [31]. Figure 5(e) is a CARS image at the on-resonant frequency which was obtained after removing the tip from the sample. The CARS signal was not detected in the CARS image without the silver tip, which confirms that the CARS polarization is effectively induced by the tip-enhanced field. It can be found that there exists background light in the presence of the tip, as is obvious from Fig. 5(d). This background light is emitted from the silver-coated tip. The tip emits light at the same frequency as the CARS ($2\omega_1 - \omega_2$) by the third-order nonlinear susceptibility of silver, which is attributed to local four-wave mixing (FWM). In addition, noble metals such as gold and silver generate white light continuum (WLC) which is induced by multi-photon excited photoluminescence due to recombination radiation between electrons near Fermi level and photoexcited holes in the d band [32,33]. These two components become background light and compete with the CARS process. In our experiments the dominant background source is the FWM emission as the monochromator was utilized to selectively detect the signal at $2\omega_1 - \omega_2$. The background light can be seen at both the on-resonant and off-resonant frequencies, as they are independent of the molecular vibrations of the sample. Such light emission from a metallic tip degrades the image contrast and signal-to-noise ratio, and subsequently limits the smallest number of molecules that can be observed. In this experiment, however, the tip-enhanced CARS signal intensity largely surpasses the background because the number of molecules in the excited volume is enough to induce the signal.

In order to assess the spatial resolution and the capability of the sensitivity of the tip-enhanced CARS microscopy, we prepared a DNA network of poly(dA-dT)-poly(dA-dT) [34]. DNA (poly(dA-dT)-poly(dA-dT)) dissolved in water ($250\text{ }\mu\text{g/ml}$) was mixed with MgCl_2 (0.5 mM) solution, then the DNA solution was cast on a coverslip and blow-dried after the fixation time of ~ 2 hours. Mg^{2+} has a role for the linkage between DNA and oxygen atoms of the glass surface. Figure 6(a) shows a typical topographic image of the DNA network sample. The DNA network consists of bundles of DNA double-helix filaments aligned parallel on the glass substrate. Since the diameter of single DNA double-helix filaments

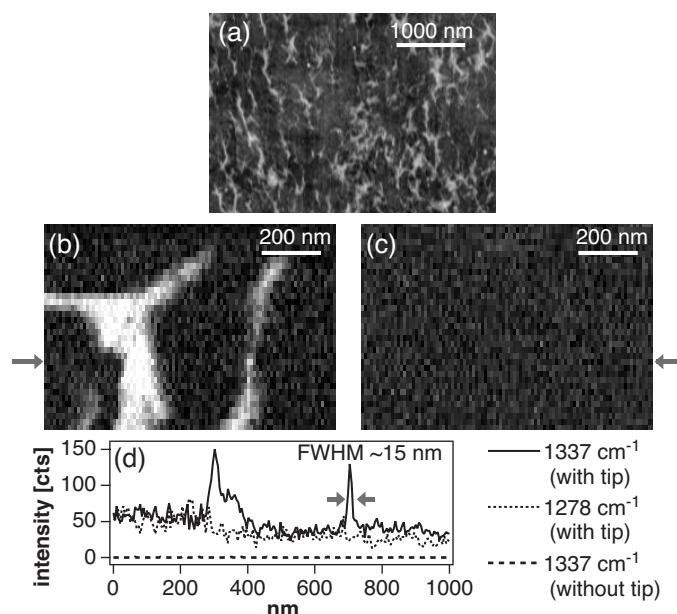


Fig. 6. CARS images of the DNA network. (a) Topographic image of the DNA network. (b) Tip-enhanced CARS image at on-resonant frequency (1337 cm^{-1}). (c) Tip-enhanced CARS image at the off-resonant frequency (1278 cm^{-1}). (d) One dimensional line profiles of the row indicated by the solid arrows. The scanned area is 1000 nm by 800 nm . The number of photons counted in 100 ms was recorded for one pixel. The acquisition time was ~ 12 minutes for the image. The average powers of the ω_1 and ω_2 beams were $45\text{ }\mu\text{W}$ and $23\text{ }\mu\text{W}$ at the 800 kHz repetition rate.

is $\sim 2.5\text{ nm}$, the height of the bundle structures is $\sim 2.5\text{ nm}$, and the width is from 2.5 nm (for single filaments) to a few tens of nanometers (for ca. 10 filaments). The CARS images at the on- and off- resonant frequencies are shown in Figs. 6(b) and (c). The DNA bundles are observed at the resonant frequency in Fig. 6(b), while they cannot be visualized at the off-resonant frequency in Fig. 6(c). This indicates that the observed contrast is dominated by the vibrationally resonant CARS signals. Figure 6(d) shows one-dimensional profiles of the row indicated by solid arrows, which were acquired with a $\sim 5\text{ nm}$ step. The line profile acquired without the silver tip is also added for comparison. Only the CARS profile with the tip in the on-resonant condition has peaks at the positions of $x \sim 370\text{ nm}$ and $x \sim 700\text{ nm}$ where adenine molecules exist in the DNA double helix, while the other line profiles do not sense the existence of the molecules. The full width of half maximum of the right peak is found to be $\sim 15\text{ nm}$, as indicated in Fig. 6(d). This spatial resolution is much better than our previous works using spontaneous Raman scattering, which can be attributed to the nonlinearity of the CARS process.

The size of the locally excited volume of the DNA structure is estimated to be ~ 1 zeptolitre. For the estimation of the excited volume, we assume the tip-enhanced local excitation spot to be a sphere with 20 nm diameter centered at the tip end in which the excitation efficiency is uniform. The locally excited volume is defined as the volume overlapped by the excitation spot and the sample. In these assumptions, the excited volume is approximately a column with 2.5 nm height and 20 nm diameter. We also estimated the intensity enhancement factor of the CARS intensity is estimated to be of the order of $\sim 10^6$. For the estimation of enhancement factor we preliminarily measured CARS intensity of a DNA cluster without the silver tip, then estimated the efficiency of the CARS emission per unit volume, peak power and repetition rate. Using the estimated efficiency, we derived the enhancement factor. The estimated enhancement factor for the CARS intensity ($\sim 10^6$) leads to the enhancement factor of ~ 100 for each excitation field. This factor is

quite realistic and reasonable, as compared to previous numerical results [35,36], although this estimation is very much subject to the changes in each parameter with high-order dependency. The smallest detectable volume of DNA under the current experimental condition is estimated as $\sim 1/4$ zeptolitre, which is derived from the signal-to-noise ratio of $\sim 15:1$ in Fig. 6(d) and the quadratic dependence of the CARS intensity on interaction volume. This indicates that our CARS microscope is capable of sensing a vibrational-spectroscopic signal from an enormously small subzeptolitre volume.

5. CONCLUSIONS

We have successfully visualized the DNA nanostructures by the CARS microscope using a silver coated probe. Spatial resolution has been much improved by the use of tip-enhanced near field, as compared to the far-field (diffraction-limited) CARS microscopy. The spatial resolution is found better rather than tip-enhanced linear Raman microscopy, which is attributed to the strong confinement of the CARS generation owing to its third-order nonlinearity besides the near-field enhancement by the tip.

REFERENCES

1. Y. Inouye and S. Kawata, *Opt. Lett.* **19**, 159 (1994).
2. S. Kawata (Ed.) *Near-Field Optics and Surface Plasmon Polaritons*; Springer: Berlin (2001).
3. N. Hayazawa, Y. Inouye, and S. Kawata, *J. Microsc.* **194**, 472 (1999).
4. H. F. Hamman, A. Gallagher, and D. J. Nesbitt, *Appl. Phys. Lett.* **76**, 1953 (2000).
5. E. J. Sánchez, L. Novotny, and X. S. Xie, *Phys. Rev. Lett.* **82**, 4014 (1999).
6. A. Lahrech, R. Bachelot, P. Gleyzes, and A.C. Boccarda, *Opt. Lett.* **21**, 1315 (1996).
7. B. Knoll, and F. Keilmann, *Nature* **399**, 134 (1999).
8. T. Masaki, K. Goto, Y. Inouye, and S. Kawata, *J. Appl. Phys.* **95**, 334 (2004).
9. Y. Inouye, N. Hayazawa, K. Hayashi, Z. Sekkat, and S. Kawata, *Proc. SPIE* **1791**, 40 (1999).
10. R. M. Stöckle, Y. D. Suh, V. Deckert, and R. Zenobi, *Chem. Phys. Lett.* **318**, 131 (2000).
11. M. S. Anderson, *Appl. Phys. Lett.* **76**, 3130 (2000).
12. N. Hayazawa, Y. Inouye, Z. Sekkat, and S. Kawata, *Opt. Commun.* **183**, 333 (2000).
13. N. Hayazawa, Y. Inouye, Z. Sekkat, and S. Kawata, *Chem. Phys. Lett.* **335**, 369 (2001).
14. N. Hayazawa, T. Yano, H. Watanabe, Y. Inouye, and S. Kawata, *Chem. Phys. Lett.* **376**, 174 (2003).
15. A. Hartschuh, E. J. Sanchez, X. S. Xie, and L. Novotny, *Phys. Rev. Lett.* **90**, 95503 (2003).
16. Y. R. Shen, *The Principles of Nonlinear Optics*; Wiley: New York (1984).
17. M. D. Levenson, and S. S. Kano, *Introduction to Nonlinear Optical Spectroscopy*, Academic Press, Orlando (1988).
18. T. Ichimura, N. Hayazawa, M. Hashimoto, Y. Inouye, and S. Kawata, *Appl. Phys. Lett.* **84**, 1768 (2004).
19. N. Hayazawa, T. Ichimura, M. Hashimoto, Y. Inouye, and S. Kawata, *J. Appl. Phys.* **95**, 2676 (2004).
20. T. Ichimura, N. Hayazawa, M. Hashimoto, Y. Inouye, and S. Kawata, *Phys. Rev. Lett.* **92**, 220801 (2004).
21. R. D. Schaller, J. Ziegelbauer, L. F. Lee, L. H. Haber, and R. J. Saykally, *J. Phys. Chem. B* **106**, 8489 (2002).
22. A. Zumbusch, G. R. Holtom, X. S. Xie, *Phys. Rev. Lett.* **82**, 4142 (1999).
23. M. Hashimoto, T. Araki, and S. Kawata, *Opt. Lett.* **25**, 1768 (2000).
24. M. Hashimoto, and T. Araki, *J. Opt. Soc. Am. A*, **18**, 771 (2001).
25. J.-X. Cheng, A. Volkmer, and X. S. Xie, *J. Opt. Soc. Am. B*, **19**, 1363 (2002).
26. Z. Xiaolin, and R. Kopelman, *Ultramicroscopy* **61**, 69 (1995).
27. T. Ichimura, N. Hayazawa, M. Hashimoto, Y. Inouye, and S. Kawata, *J. Raman Spectrosc.* **34**, 651 (2003).
28. L. Novotny, E. J. Sánchez, and X. S. Xie, *Ultramicroscopy* **71**, 21 (1998).

29. A. Bouhelier, M. Beversluis, A. Hartschuh, and L. Novotny, *Phys. Rev. Lett.* **90**, 013903 (2003).
30. H. Watanabe, Y. Ishida, N. Hayazawa, Y. Inouye, and S. Kawata, *Phys. Rev. B* **69**, 155418 (2004).
31. B. Hecht, H. Bielefeldt, Y. Inouye, D. W. Pohl, and L. Novotny, *J. Appl. Phys.* **81**, 2492 (1997).
32. G. T. Boyd, Z. H. Yu, and Y. R. Shen, *Phys. Rev. B.* **33**, 7923 (1986).
33. J. P. Wilcoxon, and J. E. Martin, *J. Chem. Phys.* **108**, 9137 (1998).
34. S. Tanaka, L. T. Cai, H. Tabata, and T. Kawai, *Jpn. J. Appl. Phys.* **40**, L407 (2001).
35. H. Furukawa, and S. Kawata, *Opt. Commun.* **148**, 221 (1998).
36. J. T. Krug II, E. J. Sánchez, and X. S. Xie, *J. Chem. Phys.* **116**, 10895 (2002).